LATEST ACHIEVEMENTS ON ANTENNA DIAGNOSTICS AND PROCESSING OF MEASURED FIELDS

Cecilia Cappellin, Erik Jørgensen, Peter Meincke
TICRA, Læderstræde 34
1201 Copenhagen K, Denmark

Marco Sabbadini
ESTEC, European Space Research and Technology Centre, Keplerlaan 1
2201 Noordwijk, The Netherlands

ABSTRACT

A stand-alone commercial program, performing advanced electromagnetic processing of measured data, is being developed by TICRA. The program reads the measured field and computes the extreme near field or the currents on the antenna surface. From the inspection of the extreme near field or currents, the program will solve typical antenna diagnostics problems, such as identification of array element failure and antenna surface errors, but also allow artificial removal of undesired contributions, such as currents on cables and fixtures, thereby saving valuable time and resources in the antenna design and validation process. The program will be based on two field reconstruction techniques, the SWE-PWE presented at AMTA in 2007, and a new and more accurate inverse higher-order Method of Moments (INV-MoM). The paper will illustrate the theory behind the two techniques and present numerical cases with simulated data.

Keywords: antenna diagnostics, source reconstruction, holography, inverse source problem, electromagnetic algorithms.

1. Introduction

The interest in techniques able to identify electrical and mechanical errors affecting an antenna under test (AUT) only on the basis of the radiated field has grown extensively in the latest years. Numerous groups in Europe and US have developed algorithms, generally identified by the common name of antenna diagnostics techniques, to reach this purpose, see for example [1]-[3] and [8]-[11].

The works presented in [1]-[2] are based on the well-established relation between the visible region of the plane wave spectrum and the antenna far-field pattern [4]. Through the inverse Fourier transform of the plane wave spectrum the antenna extreme near-field is obtained. The technique, often called backward transformation, is applicable to general antennas and is simple and computationally efficient due to the use of the inverse fast Fourier transform. The major drawback of the backward transformation is that the invisible region of the plane-wave spectrum is neglected. This results in inaccurate extreme near fields, especially for low directivity antennas, and in a spatial resolution of the extreme near field limited to half a wavelength.

The inverse Method of Moment technique [8]-[11] allows reconstruction of the equivalent currents on an arbitrary surface enclosing the AUT based on full-sphere or truncated measured fields. The technique is normally more computationally demanding than the backward transformation and therefore only applicable to small and medium sized antennas. The accuracy of the INV-MoM technique strongly depends on the choice of geometrical discretization, the choice of basis functions used in the MoM, and the chosen regularization scheme.

It is seen that the proposed antenna diagnostics techniques generally are well suited to certain types of problems but less suitable for others. Furthermore, some are limited in the accuracy that they can provide either because of the algorithm or the antenna measurement techniques on which they are based. Moreover, all the existing techniques are not available as a self-contained software program: some are meant to be embedded in a specific measurement system, while some are only used by universities.

The purpose of this work is to develop a general, accurate and efficient stand-alone commercial program for antenna diagnostics that can be applied to small as well as large antennas, providing an accuracy of the reconstructed field and currents higher than that of the traditional techniques. The program will be based on two different electromagnetic models for antenna diagnostics. The first one is the so-called SWE-PWE technique, presented at AMTA in 2007 and fully described in [5], which computes from full-sphere measurements a plane-wave expansion of the radiated field in both the visible and invisible region of the spectral domain. From the plane

wave spectrum the near field can be reconstructed on a plane in the immediate vicinity of the AUT, in a fast and efficient way with a spatial resolution that is better than half a wavelength. The second one is an improved inverse Method of Moments algorithm based on higher-order basis functions and curved geometry modeling, combined with a newly developed regularization scheme. This method also provides a spatial resolution better than half a wavelength but the memory requirement grows rapidly with the electrical size of the antenna.

The paper is organized as follows: In Section 2 the theory behind the SWE-PWE technique is briefly summarized, while Section 3 deals with the theoretical foundation of the new INV-MoM algorithm. In particular, Section 3.1 focuses on discretization, Section 3.2 on regularization, and Section 3.3 on the obtainable resolution. A summary is finally given in Section 4.

2. The SWE-PWE Technique

The SWE-PWE technique is based on the transformation of the spherical wave expansion (SWE) to the plane-wave expansion (PWE). In practice, the SWE is generally obtained from a full sphere measurement of the radiated field. The SWE of the electric field $\vec{E}$ radiated by an antenna circumscribed by a minimum sphere of radius r_o, and valid for $r > r_o$ is given by [6],

$$\vec{E}(\vec{r}) = \frac{k}{\sqrt{\eta}} \sum_{n=1}^{\infty} \sum_{m=-n}^{n} Q_{1mn}^{(3)} \vec{F}_{1mn}^{(3)}(\vec{r}) + Q_{2mn}^{(3)} \vec{F}_{2mn}^{(3)}(\vec{r}) \quad (1)$$

where $Q_{1mn}^{(3)}$ and $Q_{2mn}^{(3)}$ are the expansion coefficients and $\vec{F}_{1mn}^{(3)}(\vec{r})$ and $\vec{F}_{2mn}^{(3)}(\vec{r})$ are the power-normalized spherical vector wave functions. The medium intrinsic admittance is η, k is the wave number, and $\vec{r}$ is the position vector. In practice, the n-summation of the SWE is typically truncated at $N = kr_o + 10$ since this is sufficient for an accurate calculation of the far-field. The PWE of the same electric field $\vec{E}$ valid for $z > z_o$, with z_o being the largest z-coordinate of the source, is given by [7],

$$\vec{E}(x,y,z) = \frac{1}{2\pi} \int_{-\infty}^{\infty} \int_{-\infty}^{\infty} \vec{T}(k_x, k_y) e^{ik_z z} e^{i(k_x x + k_y y)} dk_x dk_y \quad (2)$$

where k_x, k_y are the spectral variables and $k_z = \sqrt{k^2 - k_x^2 - k_y^2}$. The plane-wave spectrum for a given z-coordinate is $\vec{T}(k_x, k_y, z) \equiv \vec{T}(k_x, k_y) e^{ik_z z}$. The spectral domain is divided into two regions, the visible region,

for $k_x^2 + k_y^2 \le k^2$, which contains the propagating plane waves, and the invisible region, for $k_x^2 + k_y^2 > k^2$, which contains the evanescent plane waves, see Fig. 1. The two variables k_x and k_y are real, while k_z is real in the visible region but purely imaginary with a positive imaginary part in the invisible region. In practice, the k_x- and k_y-integrals are truncated at finite values $\pm k_{xmax}$ and $\pm k_{ymax}$ respectively, providing a spatial resolution (δ_x, δ_y) in the aperture field equal to $\delta_x = \pi / k_{xmax}, \delta_y = \pi / k_{ymax}$. At the border between the visible and invisible regions $k_z = 0$ and the PWE generally possesses a singularity [7].
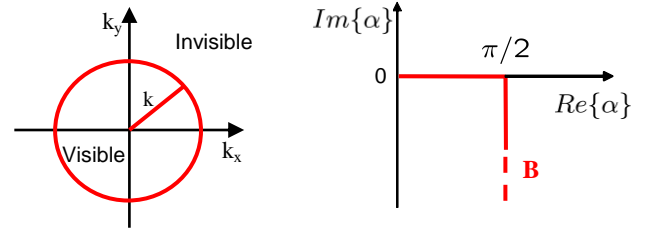
Figure 1- Visible and invisible regions of the spectral $k_x k_y$-domain (to the left), and contour B of the variable α (to the right).

It can be shown [5] that the SWE of Eq. (1) can be rigorously transformed into the PWE of Eq. (2), allowing the plane-wave spectrum $\vec{T}(k_x, k_y, z)$ to be written as

$$\vec{T}(k_x, k_y, z) = \sum_{n=1}^{\infty} \sum_{m=-n}^{n} Q_{1mn}^{(3)} \vec{T}_{1mn}(k_x, k_y, z) + \\ + Q_{2mn}^{(3)} \vec{T}_{2mn}(k_x, k_y, z) \quad (3)$$

where

$$\vec{T}_{1mn}(k_x, k_y, z) = \frac{e^{ik_z z}}{k_z} \frac{(-i)^{n+1}}{\sqrt{\eta}\sqrt{n(n+1)}} \vec{Y}_n^m(\alpha, \beta) \quad (4)$$

$$\vec{T}_{2mn}(k_x, k_y, z) = \frac{e^{ik_z z}}{k_z} \frac{(-i)^{n}}{\sqrt{\eta}\sqrt{n(n+1)}} \hat{k} \times \vec{Y}_n^m(\alpha, \beta) \quad (5)$$

with $\hat{k} = \vec{k} / k = (k_x \hat{x} + k_y \hat{y} + k_z \hat{z}) / k$. The function $\vec{Y}_n^m(\alpha, \beta)$ is the vector spherical harmonics [5], $\alpha \in B$, see Fig. 1, and is equal to $\alpha = \text{acos}(k_z / k)$, while $\beta \in [-\pi, \pi]$ and is equal to $\beta = \text{atan}(k_y / k_x)$. Equation (3) shows that the plane-wave spectrum on any z-plane $z > z_o$ can be expressed in both the visible and invisible region

as a series of the same type and with the same Q coefficients of the SWE of Eq. (1), where the only difference lies in the basis functions that are now the vector spherical harmonics instead of the power-normalized spherical vector wave functions. The imaginary values of the angle α correspond to the invisible region of the $k_x k_y$-domain. The fundamental properties of the SWE-PWE transformation are described in [5], together with their theoretical as well as practical implications for antenna diagnostics applications. Here it is just recalled that the infinite series of Eq. (3) can be truncated at a finite value N. However, while the traditional $N=kr_o+10$ is sufficient to reach convergence in the visible region of the spectrum, a larger N, and thus high order modes with small values, is necessary to reach convergence in the invisible region, due to the exponential growth of the spherical harmonics in this domain [5]. An example of this behavior can be seen in Fig. 3, showing the plane wave spectrum $\vec{T}$ at $z=0.2\lambda$ computed by Eq. (3) with different truncation values N, for the five Hertzian dipoles depicted in Fig. 2.
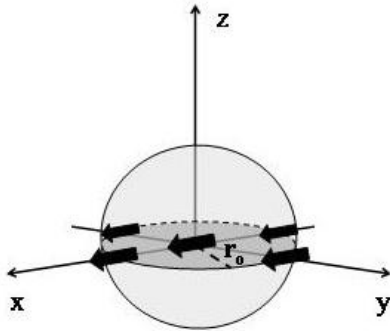
Figure 2- Five *x*-oriented Hertzian dipoles displaced on the *xy*-plane, and the minimum sphere with radius r_o.

It is seen that the plane wave spectrum can be correctly reconstructed up to $[-1.8k, 1.8k]$ in the $k_x k_y$-domain, if $N=kr_o+40=52$. This means that a large part of the invisible region is known, and thus the obtainable spatial resolution in the extreme near-field is larger than the traditional half a wavelength and equal to $\lambda/3.6$.

In practice, the finite dynamic range of the measurement system limits in general the measurement of the high order modes and thus the spectral domain where the series of Eq. (3) reaches convergence. However, it was shown [5] that for a SGH under typical measurement conditions (SNR=60 dB), the available Q coefficients were sufficient to reconstruct the visible region of the plane wave spectrum, the border for $k_z=0$, and a small part of the

invisible region, providing accurate results in the computed aperture field, see Fig. 4.
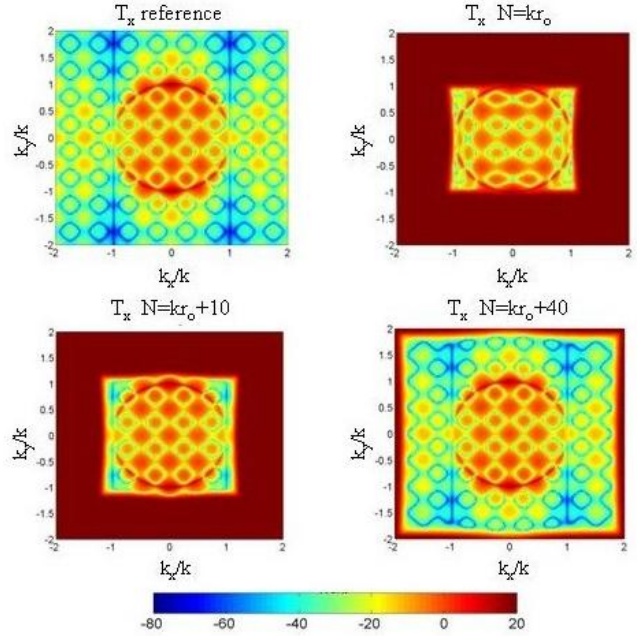
Figure 3- Amplitude of the *x*-component of the plane wave spectrum of the dipoles of Fig. 2, on $z=0.2\lambda$: first the reference T_x, then the result of Eq. (3) with $N=kr_o=12$, $N=kr_o+10=22$ and finally $N=kr_o+40=52$.
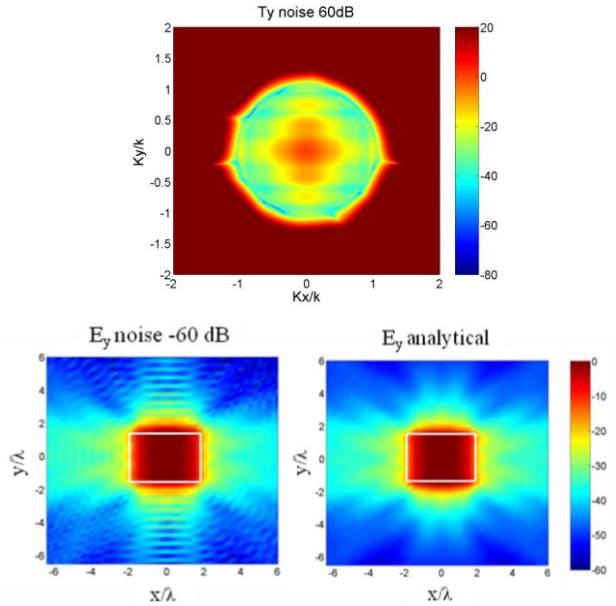
Figure 4- On top: Amplitude of the *y*-component of the spectrum $\vec{T}$ computed by Eq. (3) on $z=0.2\lambda$ with $N=kr_o+3$ and 60 dB noise. At the bottom: Amplitude of the corresponding *y*-component of the field $\vec{E}$ on the same *z*-plane and comparison with the analytical field. The white line indicates the physical aperture of the SGH.

3. The INV-MoM Technique

The INV-MoM technique solves the inverse source problem in which the tangential electric and magnetic fields on a reconstruction surface S enclosing the AUT are reconstructed from fields measured at points outside the surface. On the reconstruction surface, the equivalent electric and magnetic surface current densities to be reconstructed are

$$\vec{J}_S = \hat{n} \times \vec{H} \tag{6}$$

$$\vec{M}_S = -\hat{n} \times \vec{E} \tag{7}$$

where $\vec{E}$ and $\vec{H}$ are the fields just outside the surface of reconstruction. These equivalent currents are those corresponding to Love's equivalence principle since they produce zero field inside S. They also correspond to the physical fields one would actually measure on S.

The measured field can be written as

$$\vec{E}^{meas}(\vec{r}) = -\eta_0\, \mathcal{L}\, \vec{J}_S + \mathcal{K}\, \vec{M}_S \tag{8}$$

where η_0 is the free-space impedance and the integral operators $\mathcal{L}$ and $\mathcal{K}$ are defined as

$$\mathcal{L}\vec{J}_S = j\omega\mu_0 \left[\int_S \vec{J}_S(\vec{r}\,')G(\vec{r},\vec{r}\,')dS' + \frac{1}{k_0^2} \int_S \nabla'_S \cdot \vec{J}_S(\vec{r}\,')\nabla G(\vec{r},\vec{r}\,')dS' \right] \tag{9}$$

$$\mathcal{K}\vec{M}_S = \int_S \vec{M}_S(\vec{r}\,') \times \nabla G(\vec{r},\vec{r}\,')dS' \tag{10}$$

where k_0 is the free-space wavenumber and the scalar Green's function $G(\vec{r},\vec{r}\,')$ is

$$G(\vec{r},\vec{r}\,') = \frac{\exp(-jk_0|\vec{r}-\vec{r}\,'|)}{4\pi|\vec{r}-\vec{r}\,'|} \tag{11}$$

Equation (8) is referred to as the data equation, since it relates the measured data $\vec{E}^{meas}$ and the unknown surface current densities $\vec{J}_S$ and $\vec{M}_S$. This inverse problem has been formulated previously by several authors, including [8]-[9]. Love's equivalent currents in Eqs. (6)-(7) constitute just one set of possible equivalent currents that radiate exactly the same field $\vec{E}^{meas}$ outside the reconstruction surface, but different fields $\vec{E}_1$, $\vec{H}_1$ inside. The data equation is thus non-unique and the desired physical current densities in Eqs. (6)-(7), corresponding to Love's equivalence principle, can only be obtained if additional a priori information is imposed. This fact was first noted by Persson et al. [10] and a more detailed treatment was presented by Araque Quijano and Vecchi

[11]. The desired currents in Eqs. (6)-(7) are obtained by enforcing the a priori information that the fields $\vec{E}_1$, $\vec{H}_1$ radiated by $(\vec{J}_S, \vec{M}_S)$ inside S must be zero [10], [11]. The formulation of the required boundary condition for the electric and magnetic fields requires extraction of a principal value contribution arising when $\vec{r} \to S$ in Eqs. (9)-(10), with the result

$$-\eta_0\hat{n} \times \mathcal{L}\vec{J}_S + \left(\hat{n} \times \mathcal{K} + \frac{1}{2}\right)\vec{M}_S = 0 \tag{12}$$

$$-\left(\hat{n} \times \mathcal{K} + \frac{1}{2}\right)\vec{J}_S - \frac{1}{\eta_0}\hat{n} \times \mathcal{L}\vec{M}_S = 0 \tag{13}$$

for $\vec{r} \in S$. The expressions of Eqs. (12)-(13) are referred to as the boundary condition equations.

3.1 Discretization

The surface of reconstruction is discretized using curved patches of up to fourth order. The electric and magnetic surface currents on each patch are expanded as

$$\vec{X} = \sum_{m=0}^{M^u}\sum_{n=0}^{M^v-1} a_{mn}^u \vec{B}_{mn}^u + \sum_{m=0}^{M^v}\sum_{n=0}^{M^u-1} a_{mn}^v \vec{B}_{mn}^v \tag{14}$$

where $\vec{X} = \vec{J}, \vec{M}$, a_{mn}^u and a_{mn}^v are unknown coefficients, M^u and M^v are the expansion orders along the u- and v-directions, and $\vec{B}_{mn}^u$ and $\vec{B}_{mn}^v$ are u- and v-directed vector basis function defined as

$$\vec{B}_{mn}^u(u,v) = \frac{\vec{a}_u}{J_S(u,v)}\tilde{P}_m(u)P_n(v) \tag{15}$$

$$\vec{B}_{mn}^v(u,v) = \frac{\vec{a}_v}{J_S(u,v)}\tilde{P}_m(v)P_n(u) \tag{16}$$

Herein, $\vec{a}_u$ and $\vec{a}_v$ are the covariant unitary vectors and $J_S(u,v) = |\vec{a}_u \times \vec{a}_v|$ is the surface Jacobian. In Eqs. (15)-(16) the polynomials $P_n(v)$ along the direction transverse to the current flow are chosen to be Legendre polynomials due to their nice orthogonality properties. In the direction along the current flow, Legendre polynomials are not appropriate since they would not allow the normal current continuity to be enforced. Instead, the modified Legendre polynomials [12] are used. The current expansion above is then inserted in the data equation of Eq. (8). In order to arrive at a matrix equation, we choose two orthogonal test vectors $(\hat{\theta},\hat{\phi})$ at each field sampling point. This readily leads to the matrix equation

$$\overline{A}x = b \tag{17}$$

where x is a vector of unknown basis function coefficients, b contains $\hat{\theta}$- and $\hat{\phi}$-components of the measured field, and $\bar{A}$ is an M × N matrix with elements representing the $\hat{\theta}$- and $\hat{\phi}$-components of the field radiated by a particular basis function. The current expansion is also inserted in the boundary condition of Eqs. (12)-(13). In order to arrive at a matrix equation, we choose the testing functions

$$\vec{T}_{mn}^{u}(u,v) = \vec{a}^{u}\tilde{P}_m(u)P_n(v) \tag{18}$$

$$\vec{T}_{mn}^{v}(u,v) = \vec{a}^{v}\tilde{P}_m(v)P_n(u) \tag{19}$$

In this expression, $\vec{a}^u$ and $\vec{a}^v$ are the contravariant unitary vectors. This testing scheme is quasi-Galerkin in the sense that the basis and testing functions span the same polynomial space on rectangular patches but not in the general case. The contravariant unitary vectors are orthogonal to the covariant unitary vectors and it was found that this choice performed better than pure Galerkin testing. By taking the inner product of the testing functions and Eqs.(12)-(13), we arrive at the matrix equation

$$\bar{L}x = 0 \tag{20}$$

where $\bar{L}$ is a P × N matrix, whose elements represent the field radiated by a particular basis function, weighted by a particular testing function. The matrix is typically chosen to be square so that P = N.

3.2 Regularization

To obtain a solution to the ill-posed problem $\min\|\bar{A}x - b\|_2$, regularization is needed by imposing a priori information about the solution. The a priori information is obtained from the fact that the desired currents on the reconstruction surface should satisfy the boundary condition, that is, $\|\bar{L}x\|_2$ obtained from Eqs. (12)-(13) should be small. A regularization method suitable for this purpose is that by Tikhonov, in which the regularized solution x_λ is determined by solving the least squares problem [13]:

$$\min\left(\|\bar{A}x - b\|_2^2 + \lambda^2\|\bar{L}x\|_2^2\right) \tag{21}$$

The regularization parameter λ determines the weight given to minimizing the residual norm relative to the regularization term. It should be noted that this regularization scheme is fundamentally different from those of [10]-[11], because the data equation and the boundary condition equation are used separately.

If λ = 0 is used in the above expression, no regularization is applied, and x_0 equals the standard least-squares problem, which is useless since it is dominated by rapid oscillations due to noise. When λ^2 is increased, more weight is put to the regularization term and $x_\infty = 0$ in case $\bar{L}$ has full rank. A method for obtaining the optimum regularization parameter is the L-curve method [14]. The key idea in this method is to realize that the solution norm $\eta = \|\bar{L}x_\lambda\|_2$, plotted versus the residual norm $\delta = \|\bar{A}x_\lambda - b\|_2$ as function of λ in a logarithmic scale, is a monotonically decreasing function and forms the shape of an L. When λ is large, the solution is over-regularized, and (η, δ) is on the lower-left part of the L-curve. Similarly, when λ is small, (η, δ) is on the upper-right part. The optimum value of λ is that corresponding to the L-curve corner.

3.3 Resolution

To illustrate that the proposed INV-MoM technique is capable of reconstructing fields with a resolution better than λ0/2, a numerical case involving an array of three *y*-polarized Huygen's sources located in the *xy*-plane is considered, as shown in Fig. 5. The separation distance *d* equals λ0/4, the reconstruction surface is a box of height λ0/5, and the field is observed on the top face of the box, which is at *z* = 0.1λ0. The surface of reconstruction is discretized using 16 patches and the number of unknowns and the required number of far field sampling points are listed in Table I.
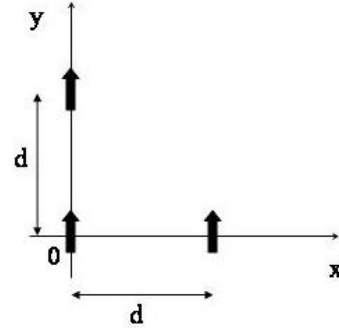
Figure 5 - Three Huygen's sources separated by the distance $d= \lambda_0/4$.

Reconstruction surface	$\lambda_0/2 \times \lambda_0/2 \times \lambda_0/5$
Patches	16
Polynomial order	5
Unknowns	1440
Far-field sampling points	720

Table I - Parameters for the considered numerical case.

The electric field on the $z = 0.1\lambda_0$ plane exhibits a rapid

variation and even the best-possible approximation with the given set of basis functions may not be an accurate representation of the exact field. To illustrate this, we show both the exact field and the best possible approximation with the current set of basis functions. The latter solution has been obtained by forward MoM. All plots in this section show the y-component of the electric field.

The results for a separation of $\lambda_0/4$ are presented in Figure 6. It can be seen in Figure 6b that the 5th-order polynomial expansion has problems along the horizontal center line. This problem can be recognized in the reconstructed field for noise-less far field data which is shown in Figure 6c. The reconstructed field is in good agreement with the best possible field for the present discretization, although the three sources appear slightly closer together. The reconstructed field for noisy far field data is shown in Figure 6d. The two lower sources can no longer be distinguished whereas the third source can clearly be identified.
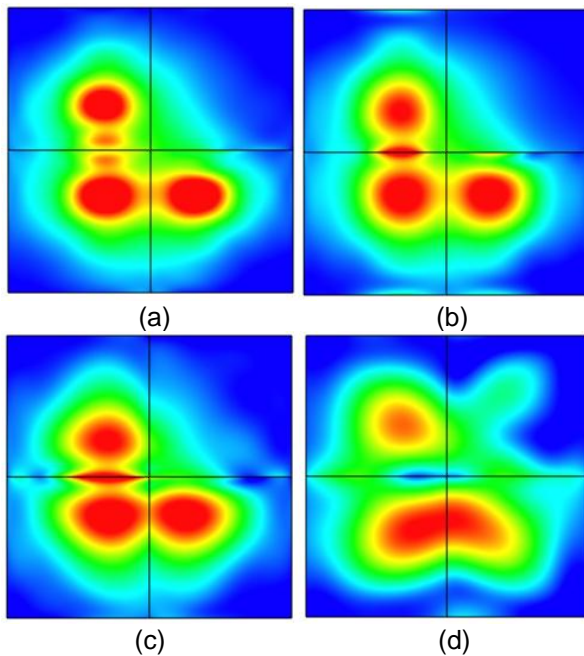
Figure 6 - Electric field from three Huygen's sources of Fig. 5 separated by a distance of $\lambda_0/4$. (a) The reference field. (b) The best possible field for the present discretization. (c) Field reconstructed from far field data without noise. (d) Field reconstructed from far field data with signal to noise ratio 60 dB.

4. Summary

Two antenna diagnostics techniques are presented, both allowing the reconstruction of currents or fields on a reconstruction surface close to the antenna with a resolution better than $\lambda_0/2$. This important property, which cannot be obtained by the traditional backpropagation-based reconstruction techniques, is illustrated through numerical examples. The two techniques are presently being implemented in a commercial computer program to be available in the nearest future.

5. References

[1] J. J. Lee, E. M. Ferren, D. P. Woollen, K. M. Lee, "Near-field probe used as a diagnostics tool to locate defective elements in an array antenna", IEEE Trans. Ant. Prop. Vol. 36(6), pp 884-889, June 1988.

[2] D. J. Rochblatt, "A methodology for diagnostics and performance improvement for large reflector antennas using microwave holography", Proc. of AMTA, pp. 7-12, 1992.

[3] E. B. Joy, M. G. Guler, "High Resolution Spherical Microwave Holography", IEEE Trans. Ant. Prop., vol. 43, 464 - 472, 1995.

[4] H. G. Booker, P. C. Clemmow, "The concept of an angular spectrum of plane waves and its relation to that of polar diagram and aperture distribution", Proc. Inst. Elec. Eng. Vol. 97(1), pp 11-16, January 1950.

[5] C. Cappellin, "Antenna diagnostics for spherical near-field antenna measurements", Ph.D. thesis, ISBN 97-887911-84802, Technical University of Denmark, Ørsted-DTU, Lyngby, Denmark, September 2007.

[6] J. E. Hansen, "Spherical Near-Field Antenna Measurements", Peter Peregrinus Ltd. London, 1988.

[7] T. B. Hansen, A. D. Yaghjian, "Plane Wave Theory of Time-Domain Fields, Near-Field Scanning Applications", IEEE PRESS, 1999.

[8] Y. Alvarez Lopez, F. Las-Heras Andres, M. R. Pino, and T. K. Sarkar, "An Improved Super-Resolution Source Reconstruction Method", IEEE Transaction on Instrumentation and Measurements, vol. 58, no. 11, pp. 3855-3866, Nov. 2009.

[9] T. F. Eibert and C. H. Schmidt, "Multilevel fast multipole accelerated inverse equivalent current method employing Rao-Wilton-Glisson discretization of electric and magnetic surface currents", IEEE Trans. Antennas Propag., vol. 57, no. 4, pp. 1178-1185, 2009.

[10] K. Persson and M. Gustafsson, "Reconstruction of equivalent currents using a near-field data transformation - with radome applications," Progress in Electromagnetics Research, vol. 54, pp. 179–198, 2005.

[11] J. L. A. Quijano and G. Vecchi, "Field and source equivalence in source reconstruction on 3d surfaces," Progress in Electromagnetics Research, vol. PIER-103, pp. 67–100, 2010.

[12] E. Jørgensen, "Higher-order integral equation methods in computational electromagnetics," Ph.D. thesis, ISBN 87-91184-21-5, Technical University of Denmark, Ørsted-DTU, Lyngby, Denmark, May 2003.

[13] P. C. Hansen, "The truncated SVD as a method for regularization," BIT, vol. 27, pp. 534–553, 1987.

[14] ——, "Analysis of discrete ill-posed problems by means of the L-curve," SIAM Review, vol. 34, pp. 561–580, Dec. 1992.